Published in final edited form as:
J Neurochem. 2009 May ; 109(4): 1067–1078. doi:10.1111/j.1471-4159.2009.06028.x.

Abnormal iron metabolism and oxidative stress in mice expressing a mutant form of the ferritin light polypeptide gene

Ana G. Barbeito[*], **Holly J. Garringer**[*], **Martin A. Baraibar**[*], **Xiaoying Gao**[*], **Miguel Arredondo**[†], **Marco T. Núñez**[‡], **Mark A. Smith**[§], **Bernardino Ghetti**[*], and **Ruben Vidal**[*]

[*]*Department of Pathology and Laboratory Medicine, Indiana Alzheimer Disease Center, Indiana University School of Medicine, Indianapolis, Indiana, USA*

[†]*Laboratorio de Micronutrientes, INTA, Universidad de Chile, Santiago, Chile*

[‡]*Department of Biology, Faculty of Sciences, Cell Dynamics and Biotechnology Institute, Universidad de Chile, Santiago, Chile*

[§]*Department of Pathology, Case Western Reserve University, Cleveland, Ohio, USA*

Abstract

Insertional mutations in exon 4 of the ferritin light chain (*FTL*) gene are associated with hereditary ferritinopathy (HF) or neuroferritinopathy, an autosomal dominant neurodegenerative disease characterized by progressive impairment of motor and cognitive functions. To determine the pathogenic mechanisms by which mutations in *FTL* lead to neurodegeneration, we investigated iron metabolism and markers of oxidative stress in the brain of transgenic (Tg) mice that express the mutant human *FTL498-499InsTC* cDNA. Compared with wild-type mice, brain extracts from Tg (FTL-Tg) mice showed an increase in the cytoplasmic levels of both FTL and ferritin heavy chain polypeptides, a decrease in the protein and mRNA levels of transferrin receptor-1, and a significant increase in iron levels. Transgenic mice also showed the presence of markers for lipid peroxidation, protein carbonyls, and nitrone–protein adducts in the brain. However, gene expression analysis of iron management proteins in the liver of Tg mice indicates that the FTL-Tg mouse liver is iron deficient. Our data suggest that disruption of iron metabolism in the brain has a primary role in the process of neurodegeneration in HF and that the pathogenesis of HF is likely to result from a combination of reduction in iron storage function and enhanced toxicity associated with iron-induced ferritin aggregates in the brain.

Keywords

animal model; hereditary ferritinopathy; neuroferritinopathy

Ferritin, the main iron storage protein, plays a central role in the maintenance of cellular iron balance (Theil 1990; Harrison and Arosio 1996; Chasteen 1998). The protein is composed of 24 subunits of both ferritin heavy chain (FTH1) and ferritin light chain (FTL). The FTH1 subunit is thought to play a role in the rapid detoxification of iron, whereas the FTL subunit facilitates iron nucleation, mineralization, and long-term iron storage (Rucker *et al.* 1996). Because of its ability to participate directly as a donor or acceptor in electron transfer reactions,

Address correspondence and reprint requests to Dr. Ruben Vidal, Department of Pathology & Laboratory Medicine, Indiana Alzheimer Disease Center, Indiana University School of Medicine, 635 Barnhill Drive MSB A136, Indianapolis, IN 46202, USA. E-mail: E-mail: rvidal@iupui.edu.

iron may become toxic by the generation of highly reactive free radicals that cause lipid peroxidation, DNA strand breaks, and protein modifications that may result in cell death (Harrison and Arosio 1996). Ferritin provides a source of metabolic active iron and also serves as an oxygen free radical cytoprotective protein, storing iron that is not needed for immediate metabolic use (Theil 1990; Harrison and Arosio 1996). In addition to ferritin, intracellular iron levels are also regulated by proteins that participate in cellular iron uptake and export including the transferrin receptor-1 (TfR-1), transferrin (Trf), the natural resistance-associated macrophage protein 2 (Nramp2) also known as divalent metal transporter 1 (Dmt1), and the metal transporter protein-1 (Mtp1) which is also described as iron-regulated transporter or Ferroportin1 (Harrison and Arosio 1996; Hentze *et al.* 2004). The expression of these proteins, including ferritin, is mainly controlled at the post-transcriptional level by the activity of the iron regulatory proteins 1 and 2 (Irp1/Irp2). These are cytosolic proteins that bind to structural elements in the mRNA named iron-responsive elements (Ires) (Kühn and Hentze 1992; Kim and Ponka 1999; Eisenstein 2000). In conditions of high intracellular iron load, Irp binding to Ire sites is inhibited, leading to an increase in ferritin translation and a decrease in *TfR-1* mRNA levels, which minimize the amount of free iron (Picard *et al.* 1998). In conditions of iron deficiency, Irp binding to Ires is increased, causing the halt in the translation of ferritin and stabilization of the *TfR-1* mRNA, increasing its protein levels.

Abnormal brain iron homeostasis has been observed in common neurodegenerative diseases such as Alzheimer disease (AD) and Parkinson disease (PD) where increased brain iron levels and iron-mediated oxidative stress seem to play an important role in the disease (Connor *et al.* 1992; Perry *et al.* 2002; Berg and Youdim 2006). A more direct link between abnormal iron metabolism and neurodegeneration is observed in Friedreich ataxia, aceruloplasminemia, neurodegeneration with brain iron accumulation, and hereditary ferritinopathy (HF) or neuroferritinopathy (Curtis *et al.* 2001; Perry *et al.* 2002; Beard and Connor 2003; Vidal *et al.* 2004a; Mancuso *et al.* 2005; Berg and Youdim 2006). HF is an adult-onset autosomal dominant genetic disease caused by mutations in the coding sequence of the *FTL* gene (Vidal *et al.* 2004b). HF affects primarily the CNS presenting clinically as an extrapyramidal movement disorder accompanied by cognitive and behavioral disturbances (Curtis *et al.* 2001; Vidal *et al.* 2004a; Mancuso *et al.* 2005). Neuropathologically, HF is characterized by a severe neuronal loss in the basal ganglia, atrophy of cerebellum (CBL) and cerebral cortex (CTX), abnormal iron accumulation, and the presence of ferritin inclusion bodies (Vidal *et al.*, 2004b). To understand the pathogenic mechanisms involved in HF, we recently developed a Tg mouse model (FTL-Tg) that expresses a human *FTL* cDNA carrying the *FTL498-499InsTC* mutation found in patients with HF (Vidal *et al.* 2008). FTL-Tg mice recapitulate several clinical and neuropathological features of the disease; however, the mechanisms by which the *FTL498-499InsTC* mutation leads to neurodegeneration have not yet been elucidated. Herein, we report that expression of the polypeptide encoded by the *FTL498-499InsTC* mutation causes dysregulation of iron homeostasis and oxidative damage of proteins in the brain of FTL-Tg mice.

Materials and methods

Animals

Wild-type C57BL/6J mice (non-Tg) and homozygous FTL-Tg mice (FTL-Tg 4) expressing a human *FTL* cDNA carrying the *498–499InsTC* mutation (Vidal *et al.*, 2004a) were used. Copy number and transgene expression of FTL-Tg mice were previously reported (Vidal *et al.* 2008). The colony was maintained by crossing Tg animals to non-Tg C57BL/6J mice. The presence of the transgene was detected by PCR amplification as described (Vidal *et al.* 2008). Procedures using laboratory animals were in accordance with institutional guidelines.

Antibodies

For immunohistochemical studies, we used polyclonal antibodies against Ftl (Ab1277) that recognized only wild-type FTL (human and murine) (Vidal *et al.*, 2004a; Vidal *et al.* 2008), mutant-FTL (Ab1283) that recognized specifically the human mutant FTL protein (Vidal *et al.*, 2004a) and Fth1 (Y16, Santa Cruz Biotechnology, Santa Cruz, CA, USA) as described (Vidal *et al.*, 2004a; Vidal *et al.* 2008). The detection of the lipid peroxidation adduct, 4-hydroxy-2-nonenal (HNE) pyrrole, was carried out using anti-4-HNE (1 : 200; EMD Chemicals, Gibbstown, NJ, USA). For carbonyl detection, we used a rat anti-dinitrophenyl dinitrophenol (DNP) monoclonal antibody (1 : 100; Zymed, San Francisco, CA, USA). For western blot analysis we used anti-TfR-1 (1 : 1000; Zymed Laboratories, South San Francisco, CA, USA), anti-transferrin (Trf, 1 : 500; Santa Cruz Biotechnology), anti-Nramp2 (1 : 250; Alpha Diagnostic International, San Antonio, TX, USA), anti-Mtp1 (1 : 250; Alpha Diagnostic International), Ab1277 (1 : 500), Ab1283 (1 : 8000), anti-Fth1 (1 : 500; Abcam, Cambridge, MA, USA), anti-Histone H1 (1 : 500; Santa Cruz Biotechnology), and anti-β-actin (1 : 10000; Sigma, St. Louis, MO, USA).

Histology and immunohistochemistry

After anesthesia, mice were transcardially perfused with 0.9% saline followed by 4% paraformaldehyde fixative, and brains were post-fixed for 16 h. Alternatively, mice were perfused with saline and brains were fixed by immersion in fixative solution during 24 h at 4° C. The brains were embedded in paraffin and sectioned. After blocking endogenous peroxidase, sections were permeabilized with 0.1% Triton X-100 in phosphate-buffered saline (PBS; 10 mM phosphate, pH 7.4, 150 mM NaCl) for 15 min and blocked for 1 h with 10% goat serum, 2% bovine serum albumin, and 0.1% Triton X-100 in PBS. Primary antibodies were incubated overnight in blocking solution. Secondary antibodies, anti-rabbit, and anti-mouse biotinylated antibodies (1 : 450), were incubated for 1 h at 22°C in blocking solution, followed by streptavidin–horseradish peroxidase, 1 μg/mL (both from Jackson ImmunoResearch, West Grove, PA, USA). Development was performed with 0.5 mg/mL diaminobenzidine solution and 0.01% (v/v) hydrogen peroxide in 0.05 M Tris–HCl. Slides were counter-stained with hematoxylin and images were captured by a digital camera coupled to a Leica DM4000B microscope (Leica Microsystems, Nussloch, Germany). The specificity of each antibody was verified by omitting the primary antibody. For carbonyl detection, brains removed from mice perfused with saline were fixed by immersion in Methacarn (methanol : chloroform : acetic acid 6 : 3 : 1) at 4°C for 24 h, embedded in paraffin, and processed as described (Smith *et al.* 1998). Primary antibody was incubated overnight at 4°C in 1% normal goat serum in tris-buffered saline (TBS) followed by a secondary biotinylated goat anti-rat antibody and streptavidin–horseradish peroxidase (BD Biosciences, San Jose, CA, USA). Development of the staining was monitored under an 20× objective microscope. After 10 min, the substrate was rinsed with water and images were captured. Brain iron was visualized by a modified Perls' reaction with 3′,3′-diaminobenzidine intensification as described previously (LeVine 1991).

Western blot analysis

Cytoplasmic fractions were prepared from CTX and CBL of 8-month-old FTL-Tg (n = 6) and non-Tg (n = 6) male and female mice using the Nuclear Extract Kit (Active Motif, Carlsbad, CA, USA) following the manufacturer's procedures. Protein extracts were aliquoted and stored at −80°C until used. Hundred μg of protein was run in 4–20% or 12% denatured sodium dodecyl sulfate (SDS)–polyacrylamide gels (Pierce, Rockford, IL, USA) and transferred to nitrocellulose membranes (GE Healthcare, Piscataway, NJ, USA). Membranes were blocked for 1 h in 5% low fat-dried milk in TBS containing 0.1% Tween-20 and then incubated for 1 h with the primary antibody. After washing in TBS containing 0.1% Tween-20, the membranes were incubated with peroxidase-conjugated secondary antibody (1 : 5000; GE Healthcare) for

1 h. Membranes were developed using the ECL chemiluminescent detection system (GE Healthcare). Equal protein load was determined after reprobing the membrane using anti-β-actin antibodies. Exposed films containing blots were scanned and the densities of the bands measured using *Scion Image for Windows*, version Beta 4.0.2 (Scion Corporation; http://www.scioncorp.com). The densities of the bands were normalized against those of β-actin and the mean ratios calculated.

Determination of protein radicals using the DMPO–nitrone spin trap

Twelve- to thirteen-month-old-male FTL-Tg mice ($n = 4$) were used. Two mice were injected 48 and 24 h before perfusion with 500 mg/kg of 5,5-dimethyl-1-pyrroline *N*-oxide (DMPO, i.p.) as described (Cassina *et al.* 2008). The control group ($n = 2$) was injected with normal saline i.p. Animals were perfused with 0.9% saline, brains removed and either immersion fixed or homogenized in RIPA buffer (25 mM Tris–HCl, pH 7.6, 150 mM NaCl, 1% Nonidet P-40, 1% sodium deoxycholate, and 0.1% SDS, all from Sigma-Aldrich, St. Louis, MO, USA) containing protease inhibitors (Roche, Indianapolis, IN, USA), centrifuged, and the supernatant used for immunoprecipitation (IP) studies. For IP 50 µL of paramagnetic Dynabeads M-280 coated with sheep anti-rabbit IgG (Invitrogen Dynal AS, Oslo, Norway) were allowed to interact for 3 h at 22°C with a rabbit anti-DMPO nitrone adduct antiserum (Cayman Chemical Company, Ann Arbor, MI, USA). After incubation, unbound antibody was removed by washing the beads with PBS and 0.1% bovine serum albumin. Equal amounts of protein (750 µg) were allowed to interact with the beads overnight at 4°C. IP samples were resuspended in 50 µL sample buffer, resolved by SDS–polyacrylamide gels, and blotted using Ab1283. In the fixed tissue, the formation of DMPO-protein adducts was evidenced by polyclonal antibodies specifically recognizing DMPO–nitrone adducts (1 : 250; Alexis Biochemicals, San Diego, CA, USA).

Real time RT-PCR analysis

Total RNA was extracted from frozen CTX and CBL of 4- and 8-month-old non-Tg ($n = 8$) and FTL-Tg ($n = 8$) mice (four mice for each age group, two males and two females) using Trizol reagent (Invitrogen, Carlsbad, CA, USA) and treated with RNase-free DNase I (Invitrogen) before purification by RNeasy column (Qiagen, Valencia, CA, USA) as described (Vidal *et al.* 2008). Three µg of total RNA was used to generate the first-strand cDNA by using Superscript III (Invitrogen) and Oligo(dT) primers (Invitrogen). Real-time PCR was performed on a 7900HT Sequence Detection System (Applied Biosystems, Foster City, CA, USA). 6-carboxyfluorescein (FAM) and 6-carboxytetramethylrhodamine (TAMRA) dual-labeled probes as well as gene-specific primers were used for quantitative PCR. Murine *Fth1* (Mm00850707_g1), *TfR-1* (Mm00441941_m1), *Trf* (Mm00446708_m1), *ceruloplasmin* (*Cp*) (Mm00432654_m1), and mouse β-*actin* (Mm00607939_s1) were from Applied Biosystems. The probe and primers for the mouse *Ftl* gene were designed using the software Primer Express (Applied Biosystems) (Vidal *et al.* 2008). PCR was conducted by initial denaturation at 95°C for 10 min, followed by 40 cycles of 95°C for 15 s, and 60°C for 1 min. The relative quantification of gene expression between multiple samples was achieved by normalization against β-actin using the ΔC_T method for quantification. Samples were run by triplicates in each experiment. Statistical analysis was carried out using one-way ANOVA with GraphPad Prism version 4.03 (GraphPad Software, San Diego, CA, USA).

RNA isolation and multiplex expression analysis

Eight-month-old male FTL-Tg ($n = 3$) and non-Tg ($n = 3$) mice were anesthetized, transcardially perfused with 0.9% saline, and the brain and a liver sample removed. The CTX and CBL were microdissected and all three samples (CTX, CBL, and liver) were placed in 500 µL of RNA later (Qiagen) and frozen at −20°C. RNA was isolated from the CTX and CBL

using RNeasy Lipid Tissue Mini Kit (Qiagen) and from liver using the RNeasy Mini Kit (Qiagen) according to the manufacturer protocol. Samples were treated on column with the RNase-free DNase Kit (Qiagen) according to the manufacturer instructions. RT was performed on 50 ng of total RNA for each sample followed by multiplex PCR, and fragment separation was carried out by capillary electrophoresis using the GeXP Chemistry Protocol (Beckman Coulter, Fullerton, CA, USA). Gene-specific primer pairs (without universal tags) used in RT-PCR are listed in Table S1. Fragments were separated using a CEQ 8000 Automated Capillary DNA sequencer/Genetic Analysis Systems (Beckman Coulter) and analyzed using the GenomeLab GeXP Genetic Analysis System (Beckman Coulter) using the following fragment analysis parameters: slope threshold = 0.9999, peak height threshold = 800 rfu, peak size < 375, peak size > 150, dye = D4. Multiplex-specific fragments were selected by applying exclusion filters and the data exported to eXpress Analysis software (Beckman Coulter), where they were normalized against the mouse *polymerase II polypeptide A* (*Polr2a*) gene (Johansson *et al.* 2007). Relative mRNA level values for each of the triplicates for each sample were averaged and the mean for the replicates were compared between FTL-Tg and non-Tg mice by an unpaired two-tailed *t*-test using GraphPad Prism. Differences in relative mRNA levels with *p*-values < 0.05 were considered statistically significant. Data were reported as mean ± SD. Statistical analysis was done using GraphPad Prism version 4.03 (GraphPad Software).

Lipid peroxidation assay

Levels of HNE, which reflects lipid peroxidation, were determined in lysates from CTX and CBL using the *N*-methyl-2-phenylindole based LPO-586™ lipid peroxidation kit (Oxis International, Foster City, CA, USA) as previously described (Wong *et al.* 2001). This assay measures the level of malondialdehyde (MDA) and 4-hydroxyalkenals (4-HAE). Standard curves of MDA were established using 1,1,3,3 tetramethocypropane. To minimize non-specific oxidation during sample preparation, 5 mM butylated hydroxytoulene dissolved in acetonitrile was added to the extraction buffer. The assay was performed in duplicates using 2–3 mg of total brain lysates per reaction, and the results were calculated as picomoles of MDA + HAE per mg of protein.

Electromobility shift assay

Iron response element-binding activity was analyzed by gel retardation assay as described (Kim and Ponka 1999; Mueller and Pantopoulos 2002). Briefly, tissue samples obtained from CTX and CBL were homogenized in extraction buffer (10 mM HEPES, pH 7.5, 3 mM $MgCl_2$, 40 mM NaCl, 5% glycerol, 1 mM dithiothreitol, and 0.2% Nonidet P-40). After lysis, the samples were centrifuged for 2 min at 10 000 *g* to remove nuclei. The cytoplasmic extracts were diluted to a protein concentration of 5 mg/mL in lysis buffer without Nonidet P-40. The RNA Ire probe was transcribed *in vitro* from a linearized plasmid template (kindly provided by Dr. K. Pantopoulos) using T7 RNA polymerase in the presence of [α-^{32}P]UTP as described (Mueller and Pantopoulos 2002). For the RNA-protein complexes, 25 µg of cytoplasmic extract was incubated at 22°C with the radiolabeled ferritin Ire probe (25 000 cpm) in the absence or presence of 2% 2-mercaptoethanol (2-ME). After 10 min, heparin (50 µg) was added to the reaction to inhibit non-specific protein interactions with the probe and the incubation was continued for another 10 min. Unprotected probe was degraded by incubation with 1 U of RNase T1 for 10 min. RNA–protein complexes were analyzed in 6% non-denaturing polyacrylamide gels and visualized by autoradiography. Bands were scanned and the ratios of the intensity of the Ire–Irp complexes formed in the absence or presence of 2-ME were determined.

Non-heme iron

Non-heme iron was determined in homogenates from the CTX and CBL as described (Sohal *et al.* 1999). Briefly, 100 μL of tissue homogenate from 12-month-old non-Tg ($n = 8$) and FTL-Tg ($n = 8$) mice (four males and four females on each group) was added to an equal amount of 1.5 N HCl in a plastic microcentrifuge tube, heated at 85°C for 30 min, and centrifuged at 10 000 *g* for 5 min at 22°C. One hundred μL of the supernatant was transferred to a new plastic microcentrifuge tube, followed by the addition of 20 μL of 40% trichloroacetic acid. The reaction mixture was heated at 85°C for 15 min and centrifuged at 10 000 *g* for 5 min at 22° C. Twenty μL of the supernatant was mixed with 200 μL of 1 mM ferrozine solution [3-(2-pyridyl)-5,6-bis(4-phenylsulphonic acid)-1,2,4-triazene; Sigma-Aldrich] in 1.05 M sodium acetate (pH 4.8) and the absorbance was determined at 570 nm using a Bio-Tek 880 microplate reader (Bio-Tek Instruments, Inc., Winooski, VT, USA).

Total brain iron

Twelve-month-old non-Tg ($n = 6$) and FTL-Tg ($n = 6$) mice (three males and three females on each group) were perfused with saline, brains were rapidly removed, and immediately dissected into CTX and CBL. Brain regions were diluted 1 : 10 (wt/v) with 2-(*N*-morpholino) ethanesulfonic acid buffer and homogenized. Fifty μL of the homogenate was added to an equal volume of ultra-pure nitric acid and hydrogen peroxide, digested for 10 h at 37°C, and then further digested for 16 h at 65°C. The sample was subsequently lyophilized and later resuspended with 3.12 mM of nitric acid for iron analysis. Fe content was determined by using an atomic absorption spectrometer (AAS) equipped with graphite furnace as described (Arredondo *et al.* 2006). Calibration was against a Fe standard curve (J T Baker, Phillipsburg, NJ, USA), and MR-CCHEN-002 (Venus antiqua) and DOlt-2 (Dogfish liver) preparations were used as reference materials to validate the mineral analyses. Data were reported as the mean ± SD. Statistical analysis was performed by the unpaired Student's *t*-test using the GraphPad Prism version 4.03. Differences were declared statistically significant if $p < 0.05$.

Results

Accumulation of ferritin polypeptides in FTL-Tg mice brain

The most significant neuropathological finding in patients with HF and in FTL-Tg mice was the presence of nuclear inclusions (NIs) in neurons and glia (Vidal *et al.*, 2004a; Vidal *et al.* 2008). In FTL-Tg mice, NIs composed of the murine Ftl and Fth1 subunits and the mutated human FTL polypeptide were found throughout the CNS (Fig. 1). In the CTX of FTL-Tg mice, nuclei of many small to medium sized neurons were found to contain NIs (Fig. 1a–c). In the CBL, NIs were observed in granule cells as well as in Purkinje cells (Fig. 1d–f). Ferritin deposits could also be seen sporadically in the cytoplasm of cells containing NIs (Vidal *et al.* 2008). We prepared cytoplasmic extracts and determined ferritin levels in the cytoplasm of cells from the CTX and CBL of FTL-Tg mice by western blot analysis. A statistically significant difference between FTL-Tg mice and non-Tg controls was observed in the levels of endogenous murine Ftl and Fth1 polypeptides (Fig. 1g). Densitometric analysis showed a statistically significant ($p < 0.05$) increase in the levels of Ftl and Fth1 in the CTX of 187 ± 29.7% and 244 ± 8.5%, respectively. In the CBL, we observed an increase of 233 ± 33.6% for Ftl and of 409 ± 19.8% for Fth1 (Fig. 1h). No immunoreactivity was seen when blots were re-probed using antibodies against Histone H1 (not shown), indicating that samples were not contaminated with ferritin from NIs. The increase in ferritin protein levels was not accompanied by a statistically significant increase in the levels of *Ftl* and *Fth1* mRNAs as determined by real time RT-PCR (Fig. 1i).

Analysis of proteins involved in iron homeostasis: TfR-1, Nramp2, Mtp1, and Trf

Western blot analysis of cytoplasmic fractions revealed a statistically significant decrease in the protein levels of TfR-1 in FTL-Tg mice (Fig. 2a). Compared to non-Tg controls, protein levels of TfR-1 were decreased by 39.6 ± 11.2% in CTX and by 64.0 ± 9.1% in CBL (Fig. 2b). The change in protein levels of TfR-1 were accompanied by a statistically significant decrease in the levels of *TfR-1* mRNA. By real-time RT-PCR, we observed a decrease in the levels of *TfR-1* mRNA at 4 months of age in both, CTX and CBL of FTL-Tg mice (Fig. 2c). At 8 months of age, the levels of *TfR-1* mRNA in the CTX remained lower in FTL-Tg mice compared with non-Tg mice, although levels were not statistically significantly different in the CBL (Fig. 2d). No statistically significant differences in the protein levels of the integral membrane protein Nramp2 (also known as Dmt1 or Dct1) and the Mtp1 (Fig. 2a), as well as Transferrin (Trf) and Ceruloplasmin (Cp) (data not shown) were observed between FTL-Tg mice and wild-type controls. No statistically significant differences were observed at the mRNA levels by real-time RT-PCR for the expression of the *Cp* (Fig. 2e) and *Trf* genes (Fig. 2f).

Multiplex expression analysis

We analyzed by multiplex RT-PCR a total of 19 genes (genes and accession numbers are listed in supplementary Table 1) that play a role in iron metabolism and related pathways. Analysis was performed in triplicate and expression was normalized to the *Polr2a* as described (Johansson *et al.* 2007). The *Polr2a* gene was the most stable gene, i.e., the most reliable endogenous control. Other control genes that were analyzed were the β-*actin* (*Actb*), the *ribosomal large P0* (*Rplp0*), and the *glyceraldehyde 3-phosphate dehydrogenase* (*Gapdh*). As previously reported by real-time RT-PCR, the expression of the transgene was found to be higher in the CTX than in the CBL of FTL-Tg mice (Vidal *et al.* 2008). The expression of the *Superoxide dismutase 2* (*Sod2*) gene (but not *Sod1*) was found to be significantly increased in both CTX and CBL of FTL-Tg compared with non-Tg mice (Fig. 3). The expression of the *Irp1*, *Fth1*, and *pantothenate kinase 2* (*Pank2*) genes were significantly decreased in both the CTX and CBL of FTL-Tg mice. Interestingly, the expression of both heme oxygenase (*Hmox*) 1 and 2 genes were significantly decreased in the CBL, and non-significantly decreased in CTX of FTL-Tg mice compared with non-Tg mice. The expression of the integral membrane protein, Nramp2 (or *Dmt1*), was found to be decreased in the CBL and significantly decreased in the CTX of FTL-Tg mice. *Trf* expression was found decreased in the CBL and decreased significantly in the CTX of FTL-Tg mice. No significant changes were observed in the other genes tested. The multiplex data on the expression of the *Ftl*, *Fth1*, *Trf*, and *Cp* genes in the CTX and CBL of FTL-Tg mice were independently confirmed by real-time RT-PCR in animals of same age. As by real-time RT-PCR, mRNA levels of *TfR-1* were also found to be decreased by multiplex expression analysis, however, the values did not reach statistical significance. Unlike the expression pattern seen in the CTX and CBL, *TfR-1* mRNA expression was found to be significantly increased in the liver of FTL-Tg mice while the expression of hepcidin (*Hamp*) was significantly decreased. No expression of *Hamp* was detected in the brain.

Iron accumulation in FTL-Tg mice

Histochemical analysis using a modified Perls' method for iron (LeVine 1991) showed significant staining of neuronal cell bodies and neurites in the CTX and CBL of FTL-Tg mice compared with non-Tg mice (Fig. 4a–d). In addition, iron was detected in NIs as previously described (Vidal *et al.* 2008). A statistically significant increase in the levels of non-heme iron in FTL-Tg mice compared with non-Tg controls was observed by the colorimetric ferrozine method (Fig. 4e). A difference of 13.7% was observed in the CTX between FTL-Tg and non-Tg mice (FTL-Tg: 2.57 ± 0.18 nmol Fe/mg protein, non-Tg: 2.26 ± 0.10 nmol Fe/mg protein) and a difference of 19.3% was observed in the CBL (FTL-Tg: 3.03 ± 0.23 nmol Fe/mg protein, non-Tg: 2.54 ± 0.17 nmol Fe/mg protein). Total brain iron measured by AAS showed a non-

significant change in the total iron content in the CTX between FTL-Tg mice and non-Tg controls (FTL-Tg 269.7 ± 55.3 nmol/g wet weight, non-Tg: 221.1 ± 44.4 nmol/g wet weight) and a significant increase in the total iron content in the CBL of FTL-Tg mice (FTL-Tg 235.1 ± 14.6 nmol/g wet weight, non-Tg 213.3 ± 11.1 nmol/g wet weight).

Ire–Irp binding activity

We used the electromobility shift assay to determine differences in the Ire–Irp interaction in the CTX (Fig. 5a) and CBL (Fig. 5b) between FTL-Tg mice and non-Tg controls. Ire–Irp binding was reduced in FTL-Tg mice compared with non-Tg mice (Fig. 5). Interestingly, Ire–Irp1 binding was found to be increased in the CTX (Fig. 5a) of FTL-Tg mice but was reduced in the CBL (Fig. 5b). With each electromobility shift assay, a parallel incubation was performed that included 2-ME which promoted maximal Ire–Irp1 binding when added to the incubation mixture. Addition of 2-ME showed a decrease in the total binding activity of Irp1 (87 ± 4.1% of the non-Tg binding) in samples from the CTX of FTL-Tg mice, which was not observed in samples from the CBL (Fig. 5b), and may account for the difference in Irp1 binding observed in the CTX of FTL-Tg mice. Irp2 binding was significantly decreased in both brain regions (Fig. 5).

Evidence of oxidative stress in FTL-Tg mouse brain tissue

By immunohistochemistry, we observed an increased in the staining for HNE protein modification (which reflects lipid peroxidation) in FTL-Tg mice, particularly in NIs of the CTX and CBL (Fig. 6a–d). As lipid peroxides were unstable and decomposed to form a complex series of reactive aldehydes, we analyzed the levels of MDA and 4-HAE, two reactive products generated as a result of lipid peroxidation. The levels of MDA and 4-HAE in the CTX were found increased with statistical significance ($p < 0.05$) in FTL-Tg mice compared with non-Tg control mice. An increase in the levels of MDA and 4-HAE in the CBL of FTL-Tg mice was also observed, although it did not reach statistically significance (Fig. 6e). The presence of protein carbonyls which were considered sensitive biomarkers of oxidative stress was detected by immunohistochemistry by *in situ* 2,4-dinitrophenylhydrazine derivatization coupled with an anti-DNP antibody system. We observed the presence of DNP adducts mainly in NIs and in the perinuclear area of neurons and some glial cells in the CTX and Purkinje cells of the CBL of FTL-Tg mice but not in non-Tg controls (Fig. 6f–i). Immunohistochemical detection of protein radicals after systemic administration of DMPO to animals (Cassina *et al.* 2008) showed the presence of intense immunolabeling of DMPO radical adducts at the sites of ferritin inclusions and in the cytoplasm of many cells in DMPO-injected FTL-Tg mice (Fig. 6k and m), whereas a low background was observed in the vehicle injected FTL-Tg mice (Fig. 6j and l). IP of tissue samples from DMPO-injected FTL-Tg mice with anti-DMPO was performed and analyzed by western blotting using antibodies specific for the mutant human FTL polypeptide. We detected two bands at ~20 and ~40 kDa, corresponding to ferritin monomers and dimers, respectively (Fig. 6n).

Discussion

We have recently generated Tg mice expressing a human *FTL498-499InsTC* cDNA (Vidal *et al.* 2008) to investigate the role of mutations in the *FTL* gene in the development of HF. As in patients with HF (Vidal *et al.* 2004a), the presence of ferritin NIs was the main neuropathological finding in the CNS of FTL-Tg mice. In addition, accumulation of ferritin in the cytoplasm could also be seen sporadically by immunohistochemistry in patients with HF and in FTL-Tg mice (Vidal *et al.* 2004a; Vidal *et al.* 2008). In FTL-Tg mice, gene expression analysis of different proteins involved in iron homeostasis revealed a profile that was consistent with abnormal brain iron metabolism in Tg mice compared with control mice. Intracytoplasmic ferritin accumulation in the CTX and the CBL of Tg mice was accompanied by a significant

decrease in the levels of TfR-1 protein and mRNA, abnormal iron accumulation, a decrease in Irp binding, and the presence of oxidative damage. Our work provides *in vivo* evidence of dysregulation of iron metabolism in the pathophysiology of HF and establishes that FTL-Tg mice are a valuable model to study changes in iron homeostasis caused by mutations in the *FTL* gene.

Ferritin is known to have a cytoplasmic distribution, although small quantities of ferritin are present in human serum and CSF (Harrison and Arosio 1996). On the contrary, little is known about the presence of ferritin in the cell nucleus (Vidal *et al.* 2004b). As the main compartment involved in the regulation of iron metabolism is the cytoplasm of the cell, we studied cytoplasmic proteins involved in iron metabolism in FTL-Tg mice by western blot. In cytoplasmic fractions, we observed a significant accumulation of ferritin that was not associated with changes in the levels of murine ferritin mRNAs as determined by real time RT-PCR. Analysis of the expression of the ferritin genes by multiplex PCR in FTL-Tg and non-Tg controls showed no differences in the expression of the *Ftl* subunit and a significant reduction of *Fth1* expression in FTL-Tg mice. These data support the notion that ferritin accumulation in HF was not associated with increased transcription of the ferritin genes. The accumulation of cytoplasmic ferritin may be explained by the deposition of ferritin aggregates, similarly to what occurs in the nucleus during the course of the disease, and/or by overproduction of ferritin (enhanced translation of ferritin mRNAs) by the cells in response to the diminished iron-binding activity of mutation-containing ferritin. The mutant FTL polypeptide has a C terminus that is changed in length and primary amino acid sequence (Vidal *et al.* 2004a). The mutant polypeptide has different amino acids at residues 167 to 175 and 16 additional amino acids at residues 176 to 191. As a consequence, the mutant FTL polypeptide is predicted not to have the last α-helical domain (E helix). We have proposed that this change may have a significant impact on the structure of the FTL and the stability of the ferritin molecules (Vidal *et al.* 2004b). However, mutant FTL polypeptides can assemble spontaneously into ferritin spherical shells in a soluble manner, but these homopolymers are less stable than wild-type FTL homopolymers precipitating at iron : ferritin ratios of over 1000 iron atoms per ferritin 24-mer (Baraibar *et al.* 2008). Ferritin particles containing the mutant FTL polypeptide have a diminished ability to sequester and store mineralized iron and aggregate well before wild-type ferritin as iron levels are increased (Baraibar *et al.* 2008). Therefore, the mutant FTL polypeptide may act as a dominant negative mutant, leading to a failure of ferritin in its iron storage function and an increase in the levels of intracellular iron (Vidal *et al.*, 2004b; Baraibar *et al.* 2008; Vidal *et al.* 2008). Intracellular free iron may generate a positive feedback loop, in which it promotes the release of the Irps from the ferritin Ires, over-expression of ferritin polypeptides, and the aggregation of mutant-containing ferritin as observed in patients with HF and in FTL-Tg mice. In support of this hypothesis, we observed that the non-heme iron content in the CTX and CBL and the total iron content of the CBL of FTL-Tg mice were significantly increased compared with non-Tg control mice. Ferritin as a non-heme iron protein may be responsible for the increase of the non-heme iron given the observed increase in its cytoplasmic protein levels. Total iron levels were also increased by AAS, although in the CTX it did not reach statistical significance, perhaps because of the presence of heme-containing proteins and red cells contaminating the samples. The observed dysregulation of iron metabolism in FTL-Tg mice was also supported by the observation that TfR-1 protein levels were significantly decreased in FTL-Tg mice compared with non-Tg control mice. Transferrin receptors are predominantly expressed on neurons in the brain (Octave *et al.* 1983; Dickinson and Connor 1998) and a decrease in TfR-1 is a consistent response to iron overload within the brain (Pinero and Connor 2000). When Ire-binding proteins bind to the Ire in the 5′-untranslated region of ferritin, they inhibit translation but when Ire-binding proteins bind to the 3′-untranslated region of *TfR-1*, they stabilize the mRNA (Müllner and Kühn 1988). A decrease in the protein and mRNA levels of TfR-1 was observed in FTL-Tg mice compared with non-Tg control mice, and the increase in ferritin protein levels

strongly suggest loss of Irp binding. These data are in agreement with the data obtained in our binding assays, which suggests a diminished level of Irp binding activity to Ires.

We also found a statistically significant decrease in the levels of *Irp1* mRNA in the brain of FTL-Tg mice but we could not detect any changes in the levels of other Ire-regulated proteins such as Nramp2 and Mtp1 by western blotting. Recently, knockdown of IRP1 in HeLa cells has been shown to decrease IRE binding activity but did not affect *FTH1* and *TfR1* expression, whereas knockdown of *IRP2* marginally affected IRE binding activity but caused an increase in FTH1 and a decrease in TfR1. Knockdown of both IRPs resulted in a greater reduction of IRE binding activity and more severe perturbation of *FTH1* and *TfR1* expression compared with single IRP knockdown (Wang *et al.* 2007). In a knock-out model of Irp2 ($Irp2^{-/-}$), mice did not show any substantial changes in Nramp2 and ferroportin levels, although these mice display higher levels of iron and ferritin (Galy *et al.* 2005). Iron levels in the brain of $Fth1^{+/-}$ and wild type mice have been found to be similar, with $Fth1^{+/-}$ mice having less than half the levels of Fth1-ferritin (Thompson *et al.* 2003). Interestingly, the levels of the iron management proteins Trf, TfR-1, Ftl, Nramp2, and Cp were found to be increased in the $Fth1^{+/-}$ mice compared with wild-type mice. Additional evidence indicating that the FTL-Tg mouse brain is phenotypically mishandling iron comes from the analysis of multiple iron-associated genes. We observed a significant decrease in the levels of *TfR-1*, *Trf*, and *Nramp2* mRNAs, which are known to occur in conditions of iron overload (Theil 1990; Harrison and Arosio 1996; Thompson *et al.* 2003). The consequences of a reduction in the mRNA levels of *Pank2*, a gene associated with the development of Pantothenate kinase-associated neurodegeneration (Hallervorden-Spatz syndrome) remain to be determined as the contribution of *Pank2* to the total PanK activity and its localization in the cytosol rather than the mitochondria differentiate mouse and human Pank2 (Leonardi *et al.* 2007). The expression of both *Hmox* 1 and 2 genes were found significantly decreased in the CBL of FTL-Tg mice compared with non-Tg mice. The decrease in expression of these genes may have important consequences as *Hmox* 1 and 2 have anti-inflammatory, antiapoptotic, and antioxidant properties. Interestingly, our data on gene expression in the liver of FTL-Tg mice suggest that the mouse liver is iron deficient. In FTL-Tg mice, we observed an increase in the liver levels of *TfR-1* mRNA and a decrease in the expression of *Hamp*. Further studies are needed to determine whether the brain is functionally iron-depleted (even though iron levels are high) because the increased iron may be inaccessible.

Iron is a highly reactive metal that has been shown to mediate oxidative stress and cell death in many neurodegenerative diseases (Zecca *et al.* 2004). Of note, the clinical symptoms of HF, including tremor, ataxia, and cognitive decline, are also characteristic of other neurodegenerative disorders which display iron-containing inclusions and deposits within the CNS. Specifically, in AD, amyloid-containing plaques and neurofibrillary tangles specifically accumulate redox active iron (Smith *et al.* 1997; Sayre *et al.* 2000); in PD, Lewy bodies also show accumulated iron (Castellani *et al.* 2000) as do prion deposits in Gerstmann–Sträussler–Scheinker syndrome and variant Creutzfeld–Jakob disease (Petersen *et al.* 2005). In fact, it is likely that iron mediates some of the neurotoxicity seen in these conditions (Rottkamp *et al.* 2001) and it is therefore not surprising that these diseases all display substantial neuronal loss, apoptosis, and oxidative damage. In HF, the accumulation of ferritin with a diminished ability to sequester iron and an increase in the levels of iron should promote oxidative stress (Orino *et al.* 1999, 2001). The presence of markers of oxidative stress, such as lipid peroxidation products, oxidatively modified proteins, and protein radicals in the brain of FTL-Tg mice is an indication of the occurrence of oxidative stress in the model. Oxidative stress can impair mitochondrial function by disrupting the function of iron–sulfur cluster-containing factors. Interestingly, we found that mRNA levels of *Sod2*, an antioxidant protein that protects cells against mitochondrial superoxide, were increased in the brain but not in the liver of FTL-Tg mice. We propose that iron-mediated free radical damage may be a key mechanism of cellular

toxicity that leads to the observed neurodegeneration in HF and FTL-Tg mice (Vidal *et al.*, 2004b; Vidal *et al.* 2008). In addition, ferritin NIs and cytoplasmic aggregates may physically interfere with normal cellular functions (a gain of a toxic function). These two mechanisms may in tandem result in neurodegeneration. FTL-Tg mice represent a unique model to study the influence of iron misregulation on oxidative stress and neurodegeneration and to test the efficacy of anti-oxidant treatment strategies *in vivo*, with relevance to a number of neurodegenerative disorders associated with iron accumulation in the CNS.

Supplementary Material

Refer to Web version on PubMed Central for supplementary material.

Abbreviations used

2-ME, 2-mercaptoethanol
4-HAE, 4-hydroxyalkenals
AAS, atomic absorption spectrometer
CBL, cerebellum
Cp, *ceruloplasmin*
CTX, cerebral cortex
DMPO, dimethyl-1-pyrroline *N*-oxide
Dmt1, divalent metal transporter 1
DNP, dinitrophenyl dinitrophenol
FTH1, ferritin heavy chain
FTL, ferritin light chain
Hamp, hepcidin
HF, hereditary ferritinopathy
HNE, 4-hydroxy-2-nonenal
IP, immunoprecipitation
Ire, iron-responsive elements
Irp, iron regulatory protein
MDA, malondialdehyde
Mtp1, metal transporter protein-1
NIs, nuclear inclusions
Nramp2, natural resistance-associated macrophage protein 2
Pank2, *pantothenate kinase 2*
PBS, phosphate-buffered saline
Polr2a, *polymerase II polypeptide A*
SDS, sodium dodecyl sulfate
Sod, superoxide dismutase
TBS, tris-buffered saline
TfR1, transferrin receptor-1
Tg, transgenic

Acknowledgments

The authors are grateful to Debra Lucas, Rose Richardson, and Urs Kuederli for their technical assistance. We thank Dr. K. Pantopoulos for the pGEMI12.CAT plasmid. This study was supported by grants from the National Institute on Neurological Disorders and Stroke NS050227 (RV), the National Institute on Aging AG10133 (BG), and by ICM P05-001-F from MIDEPLAN, Chile (MTN and MA).

References

Arredondo M, Martínez R, Núñez MT, Ruz M, Olivares M. Inhibition of iron and copper uptake by iron, copper and zinc. Biol. Res 2006;39:95–102. [PubMed: 16629169]

Baraibar MA, Barbeito AG, Muhoberac BB, Vidal R. Iron-mediated aggregation and a localized structural change characterize ferritin from a mutant light chain polypeptide that causes neurodegeneration. J. Biol. Chem 2008;283:31679–31689. [PubMed: 18755684]

Beard JL, Connor JR. Iron status and neural functioning. Annu. Rev. Nutr 2003;23:41–58. [PubMed: 12704220]

Berg D, Youdim MB. Role of iron in neurodegenerative disorders. Top. Magn. Reson. Imaging 2006;17:5–17. [PubMed: 17179893]

Cassina P, Cassina A, Pehar M, et al. Mitochondrial dysfunction in SOD1G93A-bearing astrocytes promotes motor neuron degeneration: prevention by mitochondrial-targeted antioxidants. J. Neurosci 2008;28:4115–4122. [PubMed: 18417691]

Castellani RJ, Siedlak SL, Perry G, Smith MA. Sequestration of iron by Lewy bodies in Parkinson's disease. Acta Neuropathol 2000;100:111–114. [PubMed: 10963356]

Chasteen ND. Ferritin. Uptake, storage, and release of iron. Met. Ions Biol. Syst 1998;35:479–514. [PubMed: 9444767]

Connor JR, Menzies SL, St Martin SM, Mufson EJ. A histochemical study of iron, transferrin, and ferritin in Alzheimer's diseased brains. J. Neurosci. Res 1992;31:75–83. [PubMed: 1613823]

Curtis AR, Fey C, Morris CM, et al. Mutation in the gene encoding ferritin light polypeptide causes dominant adult-onset basal ganglia disease. Nat. Genet 2001;28:350–354. [PubMed: 11438811]

Dickinson TK, Connor JR. Immunohistochemical analysis of transferrin receptor: regional and cellular distribution in the hypotransferrinemic (hpx) mouse brain. Brain Res 1998;801:171–181. [PubMed: 9729367]

Eisenstein RS. Iron regulatory proteins and the molecular control of mammalian iron metabolism. Annu. Rev. Nutr 2000;20:627–662. [PubMed: 10940348]

Galy B, Ferring D, Hentze MW. Generation of conditional alleles of the murine iron regulatory protein (IRP)-1 and -2 genes. Genesis 2005;43:181–188. [PubMed: 16283625]

Harrison PM, Arosio P. The ferritins: molecular properties, iron storage function and cellular regulation. Biochim. Biophys. Acta 1996;1275:161–203. [PubMed: 8695634]

Hentze MW, Muckenthaler MU, Andrews NC. Balancing acts: molecular control of mammalian iron metabolism. Cell 2004;117:285–297. [PubMed: 15109490]

Johansson S, Fuchs A, Okvist A, Karimi M, Harper C, Garrick T, Sheedy D, Hurd Y, Bakalkin G, Ekström TJ. Validation of endogenous controls for quantitative gene expression analysis: application on brain cortices of human chronic alcoholics. Brain Res 2007;1132:20–28. [PubMed: 17188656]

Kim S, Ponka P. Control of transferrin receptor expression via nitric oxide-mediated modulation of iron-regulatory protein 2. J. Biol. Chem 1999;274:33035–33042. [PubMed: 10551872]

Kühn LC, Hentze MW. Coordination of cellular iron metabolism by post-transcriptional gene regulation. J. Inorg. Biochem 1992;47:183–195. [PubMed: 1431880]

Leonardi R, Zhang YM, Lykidis A, Rock CO, Jackowski S. Localization and regulation of mouse pantothenate kinase 2. FEBS Lett 2007;581:4639–4644. [PubMed: 17825826]

LeVine SM. Oligodendrocytes and myelin sheaths in normal, quaking and shiverer brains are enriched in iron. J. Neurosci. Res 1991;29:413–419. [PubMed: 1920537]

Mancuso M, Davidzon G, Kurlan RM, Tawil R, Bonilla E, Di Mauro S, Powers JM. Hereditary ferritinopathy: a novel mutation, its cellular pathology, and pathogenetic insights. J. Neuropathol. Exp. Neurol 2005;64:280–294. [PubMed: 15835264]

Mueller S, Pantopoulos K. Activation of iron regulatory protein-1 (IRP1) by oxidative stress. Methods Enzymol 2002;348:324–337. [PubMed: 11885287]

Müllner EW, Kühn LC. A stem-loop in the 3′ untranslated region mediates iron-dependent regulation of transferrin receptor mRNA stability in the cytoplasm. Cell 1988;53:815–825. [PubMed: 3370673]

Octave JN, Schneider YJ, Trouet A, Crichton RR. Iron uptake and utilization by mammalian cells. I. cellular uptake of transferrin and iron. Trends Biochem. Sci 1983;8:217–221.

Orino K, Tsuji Y, Torti FM, Torti SV. Adenovirus E1A blocks oxidant-dependent ferritin induction and sensitizes cells to pro-oxidant cytotoxicity. FEBS Lett 1999;461:334–338. [PubMed: 10567722]

Orino K, Lehman L, Tsuji Y, Ayaki H, Torti SV, Torti FM. Ferritin and the response to oxidative stress. Biochem. J 2001;357:241–247. [PubMed: 11415455]

Perry G, Sayre LM, Atwood CS, Castellani RJ, Cash AD, Rottkamp CA, Smith MA. The role of iron and copper in the aetiology of neurodegenerative disorders: therapeutic implications. CNS Drugs 2002;16:339–352. [PubMed: 11994023]

Petersen RB, Siedlak SL, Lee HG, et al. Redox metals and oxidative abnormalities in human prion diseases. Acta Neuropathol 2005;110:232–238. [PubMed: 16096758]

Picard V, Epsztejn S, Santambrogio P, Cabantchik ZI, Beaumont C. Role of ferritin in the control of the labile iron pool in murine erythroleukemia cells. J. Biol. Chem 1998;273:15382–15386. [PubMed: 9624120]

Pinero DJ, Connor JR. Iron in the brain: an important contributor in normal and diseased states. Neuroscientist 2000;6:435–453.

Rottkamp CA, Raina AK, Zhu X, Gaier E, Bush AI, Atwood CS, Chevion M, Perry G, Smith MA. Redox-active iron mediates amyloid-β toxicity. Free Radic. Biol. Med 2001;30:447–450. [PubMed: 11182300]

Rucker P, Torti FM, Torti SV. Role of H and L subunits in mouse ferritin. J. Biol. Chem 1996;271:33352–33357. [PubMed: 8969195]

Sayre LM, Perry G, Harris PLR, Liu Y, Schubert KA, Smith MA. *In situ* oxidative catalysis by neurofibrillary tangles and senile plaques in Alzheimer's disease: a central role for bound transition metals. J. Neurochem 2000;74:270–279. [PubMed: 10617129]

Smith MA, Harris PL, Sayre LM, Perry G. Iron accumulation in Alzheimer disease is a source of redox-generated free radicals. Proc. Natl Acad. Sci. USA 1997;94:9866–9868. [PubMed: 9275217]

Smith MA, Sayre LM, Anderson VE, Harris PL, Beal MF, Kowall N, Perry G. Cytochemical demonstration of oxidative damage in Alzheimer disease by immunochemical enhancement of the carbonyl reaction with 2,4-dinitrophenylhydrazine. J. Histochem. Cytochem 1998;46:731–735. [PubMed: 9603784]

Sohal RS, Wennberg-Kirch E, Jaiswal K, Kwong LK, Forster MJ. Effect of age and caloric restriction on bleomycinchelatable and nonheme iron in different tissues of C57BL/6 mice. Free Radic. Biol. Med 1999;27:287–293. [PubMed: 10468200]

Theil EC. The ferritin family of iron storage proteins. Adv. Enzymol. Relat. Areas Mol. Biol 1990;63:421–449. [PubMed: 2407067]

Thompson K, Menzies S, Muckenthaler M, Torti FM, Wood T, Torti SV, Hentze MW, Beard J, Connor J. Mouse brains deficient in H-ferritin have normal iron concentration but a protein profile of iron deficiency and increased evidence of oxidative stress. J. Neurosci. Res 2003;71:46–63. [PubMed: 12478613]

Vidal R, Ghetti B, Takao M, et al. Intracellular ferritin accumulation in neural and extraneural tissue characterizes a neurodegenerative disease associated with a mutation in the ferritin light polypeptide gene. J. Neuropathol. Exp. Neurol 2004a;63:363–380. [PubMed: 15099026]

Vidal R, Delisle MB, Ghetti B. Neurodegeneration caused by proteins with an aberrant carboxyl-terminus. J. Neuropathol. Exp. Neurol 2004b;63:787–800. [PubMed: 15330334]

Vidal R, Miravalle L, Gao X, Barbeito AG, Baraibar MA, Hekmatyar SK, Widel M, Bansal N, Delisle MB, Ghetti B. Expression of a mutant form of the ferritin light chain gene induces neurodegeneration and iron overload in transgenic mice. J. Neurosci 2008;28:60–67. [PubMed: 18171923]

Wang W, Di X, D'Agostino RB Jr, Torti SV, Torti FM. Excess capacity of the iron regulatory protein system. J. Biol. Chem 2007;282:24650–24659. [PubMed: 17604281]

Wong BS, Liu T, Li R, et al. Increased levels of oxidative stress markers detected in the brains of mice devoid of prion protein. J. Neurochem 2001;76:565–572. [PubMed: 11208919]

Zecca L, Youdim MB, Riederer P, Connor JR, Crichton RR. Iron, brain ageing and neurodegenerative disorders. Nat. Rev. Neurosci 2004;5:863–873. [PubMed: 15496864]

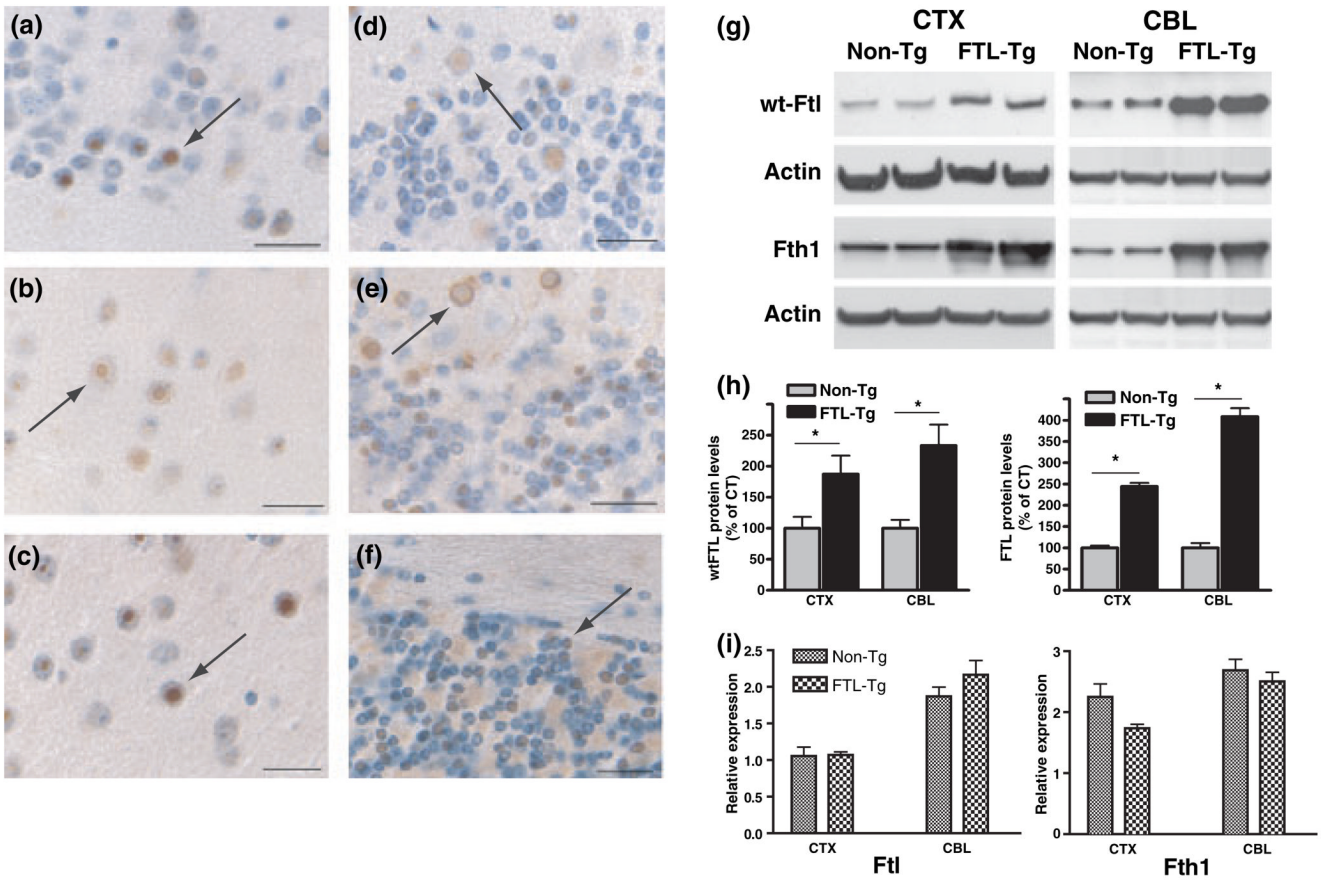

Fig. 1.

Ferritin accumulation in transgenic mice brain. Ferritin NIs in the cerebral cortex (CTX) (a–c) and in the cerebellum (CBL) (d–f) of FTL-Tg mice at 12 months of age. NIs are indicated with arrows. The levels of wild type murine Ftl and Fth1 polypeptides in the cytoplasm were determined by western blot analysis using antibodies specific for the wild type proteins (g). Membranes were reblotted for β-actin to determine equal protein loading. Densitometric analysis from two independent experiments shows a statistical significant difference between transgenic mice (FTL-Tg) and age-matched non-Tg controls (*$p < 0.05$) (h). Real-time RT-PCR analysis using RNA isolated from CTX and CBL showed no statistically significant differences in the levels of murine *Ftl* and *Fth1* mRNAs between transgenic mice and age-matched non-Tg controls (i). Immunohistochemistry was carried out using Ab1277 (a,d), Ab1283 (b,e) and Y16 (c,f). Scale bars: a–f, 20 μm. CTX and CBL of 8-month-old homozygous FTL-Tg and non-Tg mice were used for western blot and real-time RT-PCR experiments.

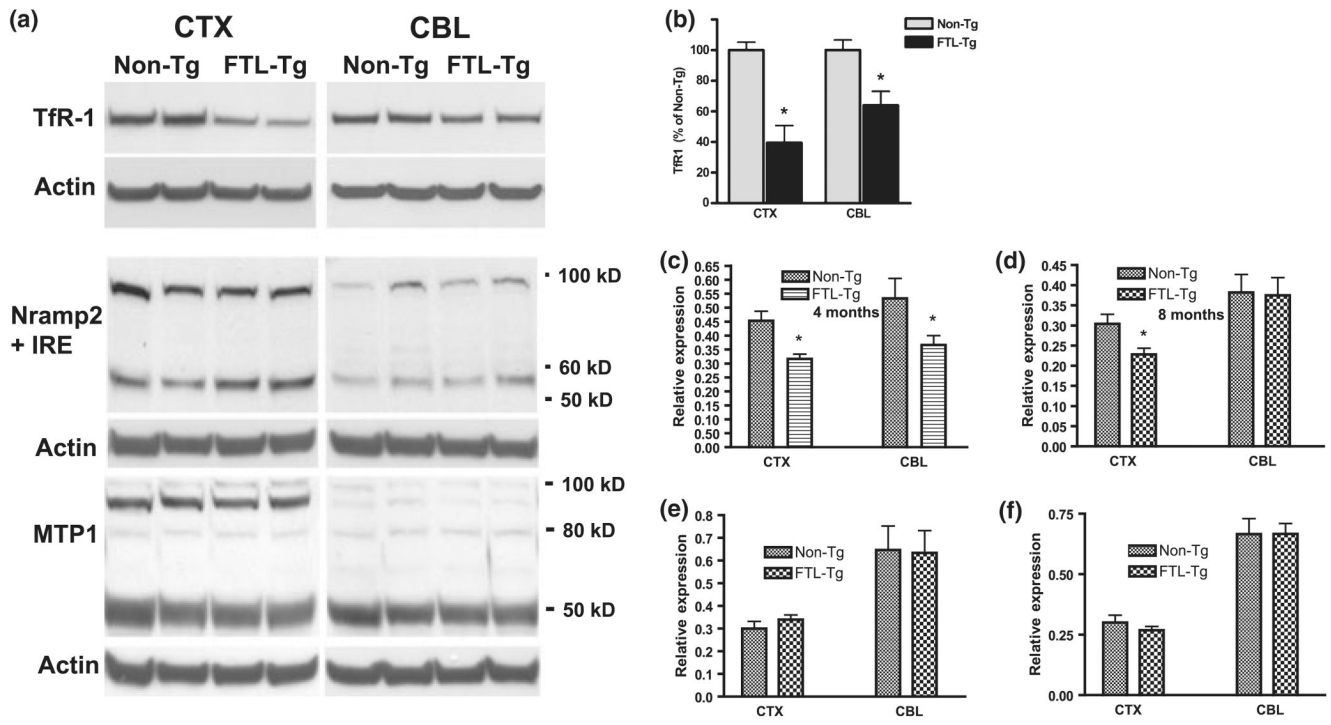

Fig. 2.

TfR-1 levels are decreased in FTL-Tg mice brain. Brain homogenates of FTL-Tg mice and non-Tg mice at 8 months of age were examined for the presence of TfR-1, Nramp2 + Ire isoform (Nramp2 + Ire) and MTP1 by western blot (a). Densitometric analysis from three independent experiments shows a statistical significant difference in the levels of TfR-1 between transgenic mice and age-matched non-Tg controls (*$p < 0.05$) (b). Real-time RT-PCR analysis shows statistically significant differences in the levels of *TfR-1* mRNA between transgenic mice and age-matched non-Tg controls at 4 (c) and 8 (d) months of age (*$p < 0.01$). No statistically significant differences were observed by real-time RT-PCR for *Cp* (e) and *Trf* (f) at 8 months of age.

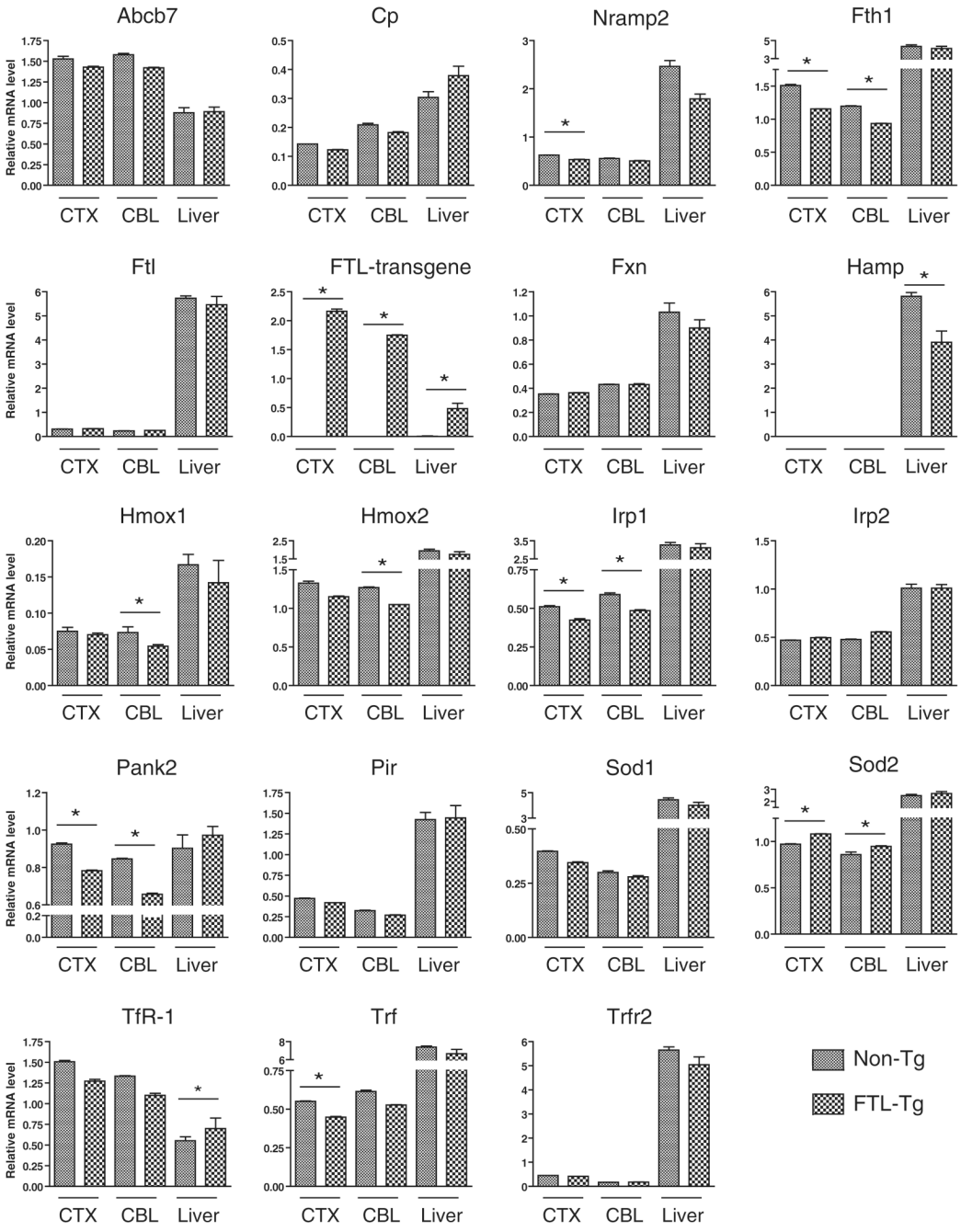

Fig. 3.

Multiplex RT-PCR expression analysis. Bar graphs depict differential gene expression levels between FTL-Tg and non-Tg control mice. Multiplex RT-PCR analysis of iron metabolism-related genes was performed on mRNA isolated from CTX, CBL, and liver. Analysis was performed in triplicate and normalized to the *Polymerase II polypeptide A* gene (*Polr2a*). The group averages are reported as relative mRNA levels mean ± SD. Genes with expression differences found to be significant ($p < 0.05$) by two-tailed *t*-test are indicated with an '*'.

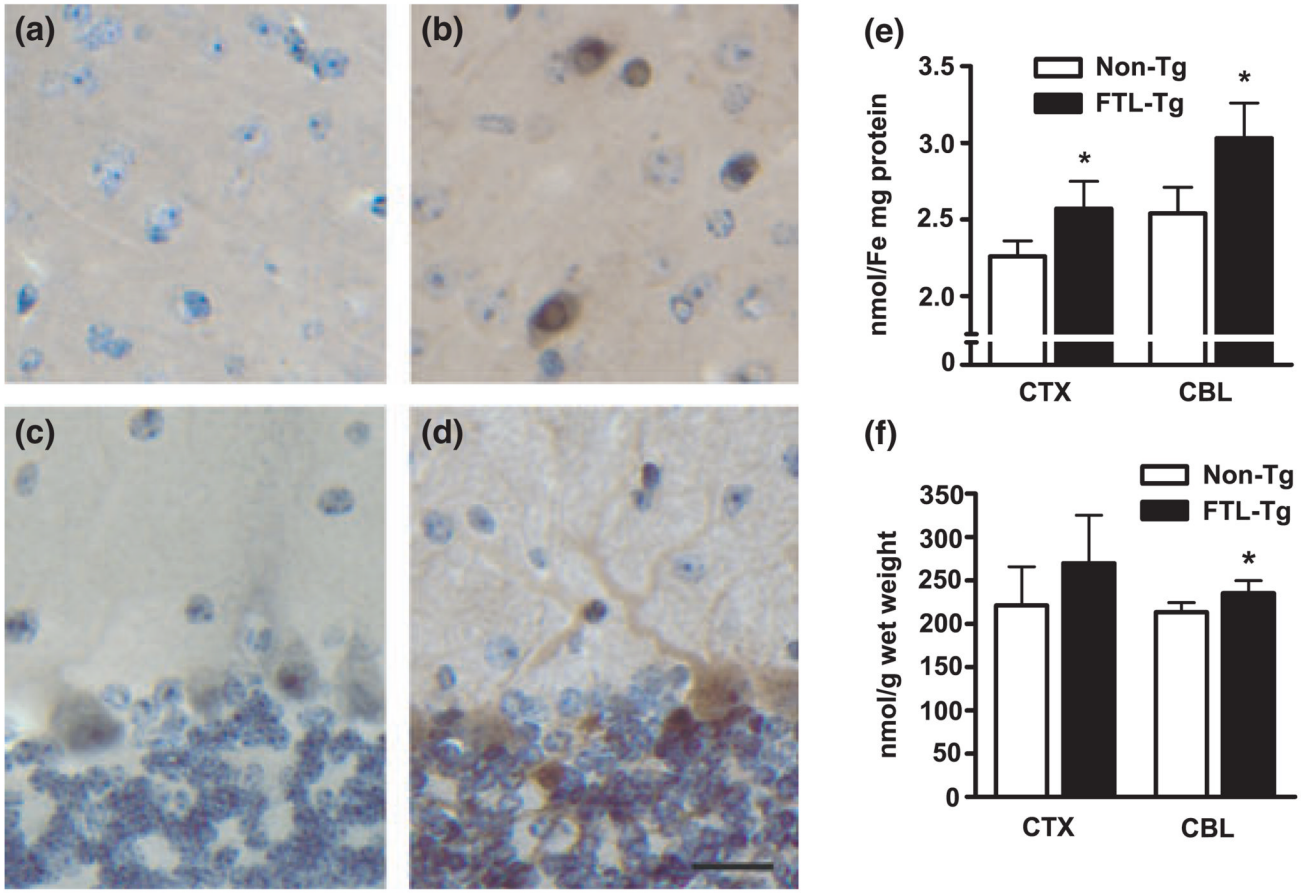

Fig. 4.

Brain iron levels in FTL-Tg mice brain. Enhanced Perls' staining was observed in sections from the cerebral cortex (a,b) and cerebellum (c,d) of 8-month-old FTL-Tg mice (b, d) compared with non-Tg controls (a, c). Iron staining was observed in NIs present in neurons of the CTX (b) and in neurons of the granule cell layer and Purkinje cells of the CBL (d), which also showed a diffuse cytoplasmic staining. A statistically significant difference in the levels of non-heme iron (nmol/mg protein) was seen in the CTX and CBL of 12-month-old FTL-Tg mice compared with non-Tg controls (*$p < 0.05$) (e). A statistically significant difference in the levels of total iron concentration (nmol/wet weight) was seen in the CBL of 12-month-old FTL-Tg mice compared with non-Tg controls (*$p < 0.05$) but not in the CTX (f).

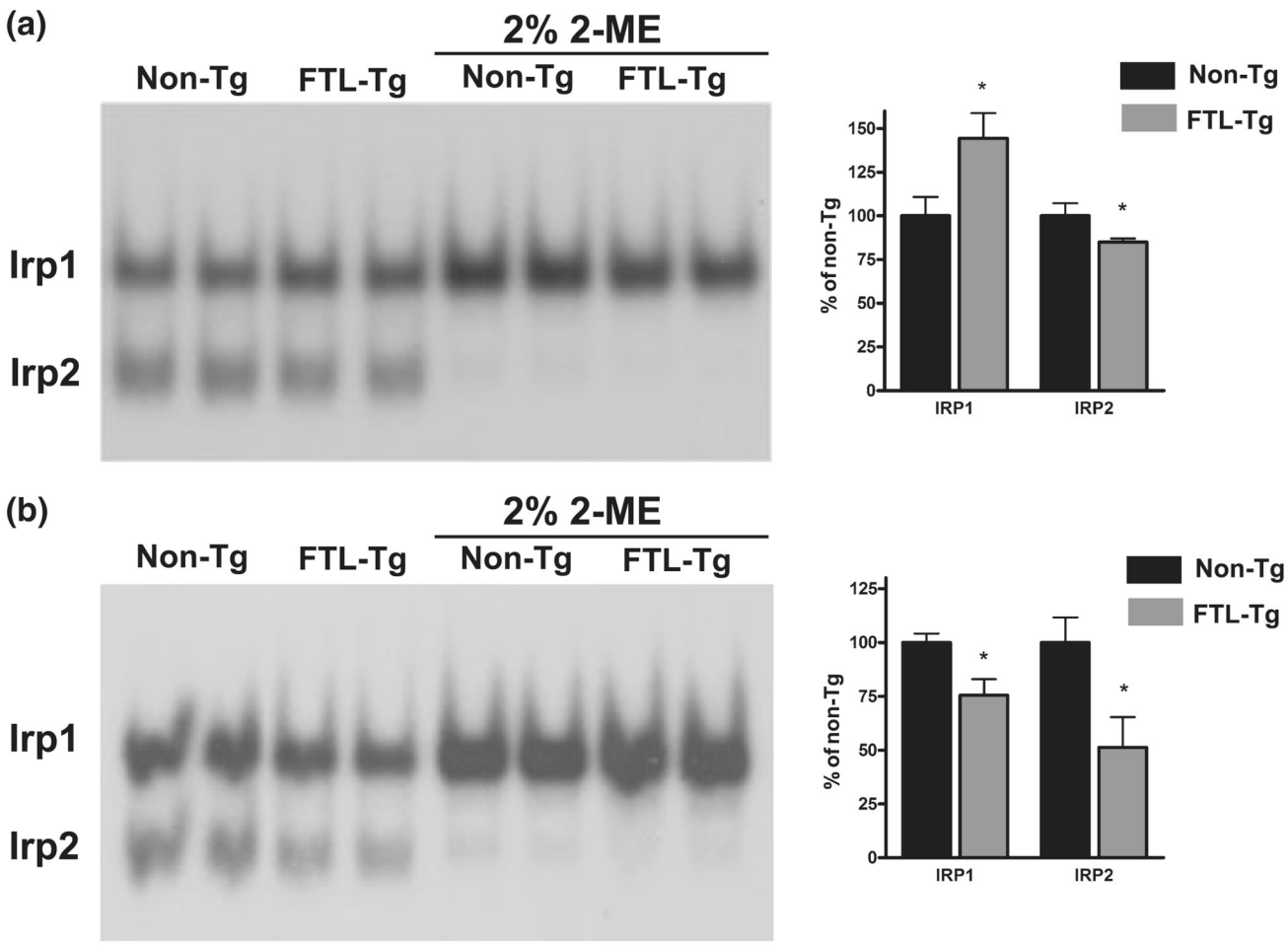

Fig. 5.

Ire-binding activities in FTL-Tg mice. Cytoplasmic extracts from non-Tg and FTL-Tg mice from CTX (a) and CBL (b) were analyzed using a gel-shift assay with a ^{32}P-labeled RNA probe containing a ferritin Ire sequence in the absence or presence of 2% 2-mercaptoethanol (2-ME). A statistically significant difference in the levels of Irp1 and Irp2 was observed between FTL-Tg mice and non-Tg controls (*$p < 0.05$).

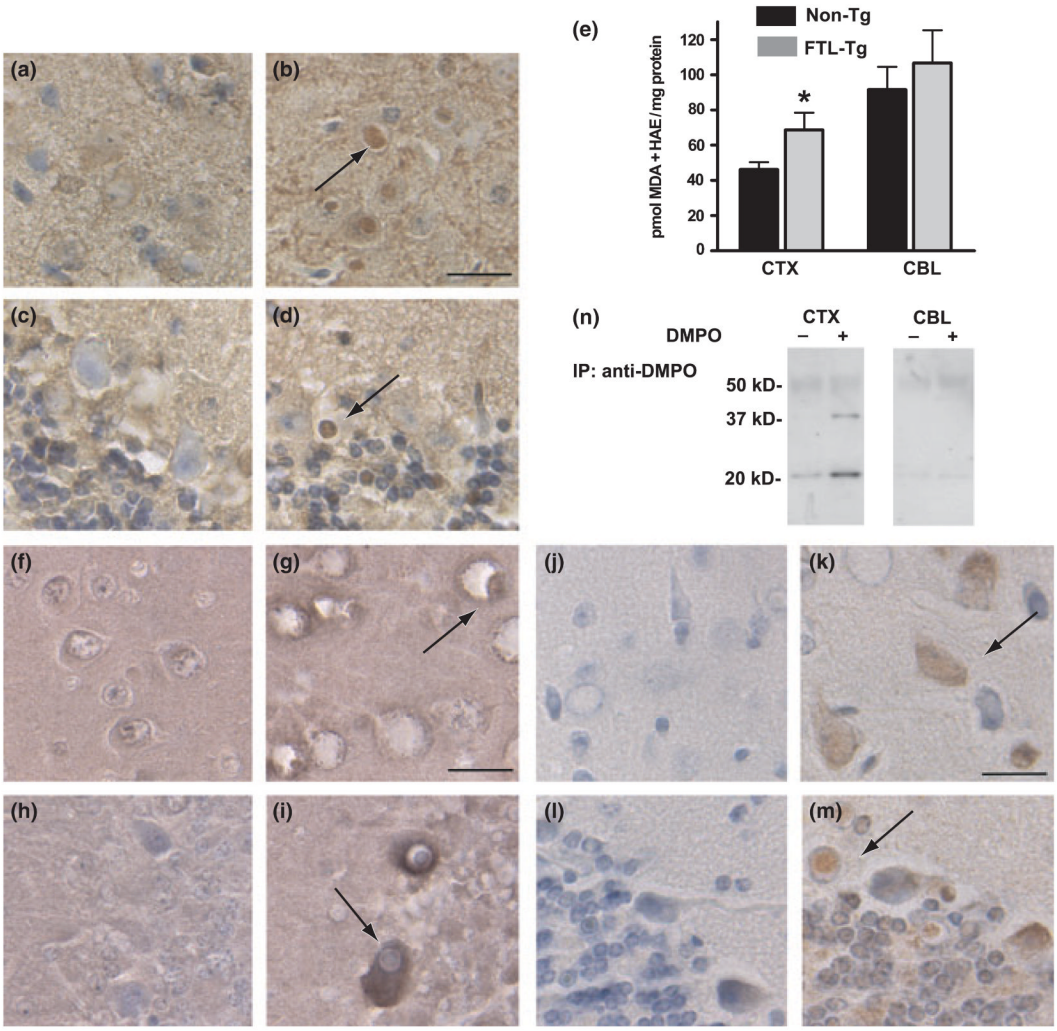

Fig. 6.

Markers of oxidative stress in FTL-Tg mice. 4-Hydroxy-2-nonenal immunoreactivity in the CTX (a,b) and CBL (c,d) of 8-month-old non-Tg controls (a, c) and FTL-Tg mice (b,d). NIs were immunolabeled by the antibody (arrows). A statistical significant difference in the concentration of the lipid peroxidation end products malondialdehyde and 4-hydroxyalkenals was observed in samples from the CTX between FTL-Tg mice and wild-type controls. Values correspond to mean ± SD (*$p < 0.05$) (e). Carbonyl immunoreactivity (arrows) in the CTX (f,g) and CBL (h,i) of 8-month-old non-Tg controls (f,h) and FTL-Tg mice (g,i). Arrows indicate intracellular immunolabeling for carbonyls in association with NIs. *In vivo* detection of protein radicals of DMPO injected FTL-Tg mice (j–m) shows immunolabeling in inclusions and cytoplasm in the DMPO-injected mice (k,m) but not in vehicle-injected transgenic animals (j,l). DMPO–ferritin adducts were observed after immunoprecipitation with anti-DMPO (n). Scale bars: a–d, f–m, 20 μm.